

H adronic I nteractions of U ltra-H igh E nergy P hotons w ith
P rottons and L ight N uclei in the D ipole P icture

T . C . Rogers and M . I . S trikman^y

D epartment of P hysics,

P ennsylvania S tate U niversity,

U niversity P ark, PA 16802, U SA

(D ated: January 26, 2020)

Abstract

We apply the dipole formalism that has been developed to describe low- x deep inelastic scattering to the case of ultra-high energy real photons with nucleon and nuclear targets. We modify the dipole model of McDermott, Frankfurt, Guzey, and Strikman (MFGS) by fixing the cross section at the maximum value allowed by the unitarity constraint whenever the dipole model would otherwise predict a unitarity violation. We observe that, under reasonable assumptions, a significant fraction of the real photon cross section results from dipole interactions where the QCD coupling constant is small, and that the MFGS model is consistent with the Froissart bound. The resulting model predicts a rise of the cross section of about a factor of 12 when the photon energy is increased from 10^3 GeV to 10^{12} GeV. We extend the analysis to the case of scattering on a ^{12}C target. We find that, due to the low thickness of the light nuclei, unitarity for the scattering on individual nucleons plays a larger role than for the scattering on the nucleus as a whole. At the same time the proximity to the black disk limit results in a substantial increase of the amount of nuclear shadowing. This, in turn, slows down the rate of increase of the total cross section with energy as compared to the proton case. As a result we find that the ^{12}C nuclear cross section rises by about a factor of 7 when the photon energy is increased from 10^3 GeV to 10^{12} GeV. We also find that the fraction of the cross section due to production of charm reaches 30% for the highest considered energies with a ^{12}C target.

PACS numbers: 12.38+t, 13.85.Tp

Keywords: QCD, Phenomenological models

E-mail: rogers@phys.psu.edu

^yE-mail: strikman@phys.psu.edu

I. INTRODUCTION

Dipole models in strong interaction physics describe the interaction of a high energy virtual photon with a hadronic target by representing the photon by a distribution over hadronic Fock states of varying sizes in the light-cone formalism. This picture has become popular for studying deep inelastic scattering in the low- x limit. It is a dipole model because the very small size configurations are usually modeled by a small quark/anti-quark pair, though larger size Fock states are not necessarily dipole configurations and should be thought of as more general hadronic states containing, for example, intrinsic gluon fields. The idea that hadrons should contain configurations interacting with different strength emerged first in the context of discussion of the inelastic diffraction [1, 2, 3]. This idea reemerged in connection with the introduction of the two gluon exchange model for the strong interaction [4, 5]. In this model the interaction of a small hadronic system with a large hadronic system is obviously proportional to the transverse size squared of this system [4]. In this context the impact parameter representation of the scattering amplitude first introduced for high energy processes by Cheng and Wu [6] in their studies of the high energy QED turned out to be useful. The relationship between the smallness of the interaction with nucleons, the small size of the incident configuration (color transparency), and Bjorken scaling was emphasized in [7] where it was demonstrated that small and large size configurations give comparable contributions to $F_2(x; Q^2)$ at small x and $Q^2 \sim \text{few GeV}^2$ – the QCD aligned jet model. The use of the eikonal model with two gluon exchange and the Cheng and Wu representation for the impact parameter photon wave function (extended to finite Q^2) was used to build a model of nuclear shadowing [8].

It was pointed out in [9] that the cross section of the dipole nucleon interaction within the leading log approximation is actually proportional to the gluon density at high virtuality and small x , resulting in a fast growth of the total cross section. The resulting dipole-nucleon cross sections were used to take into account finite Q^2 corrections to exclusive vector meson production in DIS [10]. Splitting of the dipoles into systems of dipoles was studied within the BFKL approximation in [11]. The dipole model was applied to the description of HERA DIS data by Golec-Biernat and Wustho [12] who introduced a parameterization of the dipole cross section inspired by the eikonal model which ensured that the total cross section of the interaction of dipoles of any size would reach a finite limiting value at high energies.

A more realistic model was introduced by McDermott, Frankfurt, Guzey and Strikman (MFGS) in Ref. [13]. In [13] (the MFGS model) the cross section for small dipole sizes was constrained to satisfy the perturbative QCD expression for the dipole–nucleon interaction, while for large sizes a growth consistent with the pattern of the pion–nucleon interaction was imposed. An important advantage of the model is that one can adjust the behavior of large size and small size configurations independently. The MFGS model was extended to an impact parameter analysis in Ref. [14], and other impact parameter analyses were done earlier in Ref. [15, 16].

At small Bjorken- x , the gluon distribution dominates over the quark distribution in the nucleon target, and the behavior of the small size dipole cross section is successfully predicted in leading-twist perturbative QCD (pQCD). However, at very small values of Bjorken- x , the leading-twist gluon distribution becomes unreasonably large and qualitatively new physics is expected to dominate. The usual assumption is that, whatever QCD mechanism is responsible for extremely low- x behavior, scattering of a dipole of a given size at fixed impact parameter at sufficiently high energy occurs at or near the limit allowed by unitarity. Applications of the dipole model have thus far been used mainly in searches for these qualitatively new regimes in QCD. Within the dipole picture, at fixed large Q^2 and sufficiently small x the distribution of sizes is sharply peaked around small size quark-antiquark pairs. For small photon virtualities, Q^2 , and for the energies $E = 10^3$ GeV the distribution in sizes is dominated mostly by large sizes which lie far from the pQCD regime. However, for extremely high energy photons (relevant to cosmic rays), pQCD predicts a very rapid rise in the basic cross section with an increase in dipole size. At asymptotically large photon energies, finite size configurations rapidly reach the unitarity bound and certainly lie far outside the applicability of ordinary leading-twist pQCD. Thus, we expect that for real photons with astronomically large energies, a sizable contribution to the total N cross section may arise from small size dipoles whose amplitudes in impact parameter space are close to the saturation limit for a wide range of impact parameters. To address quantitatively the issue of the real photon–nucleon or the real photon–light nucleus interaction at cosmic ray energies we need to use a model which naturally matches with pQCD for small dipole sizes as it is the small size dipoles which will play the crucial role in the analysis of maximal possible growth of the cross section. Hence we will use the MFGS model. The consistency of a particular dipole model can be checked by considering both the real photon limit and

the limit of extremely high photon energies where the total cross section should start to exhibit behavior consistent with S-channel unitarity. We will demonstrate this consistency within the MGFS model in the present paper.

There is currently an interest in the types of showers induced by ultra-high energy (UHE) cosmic ray neutrinos [17] which will be relevant to the Auger and IceCube experiments. The resulting showers are presumed to be initiated by the Bremsstrahlung photons radiated from the electron produced in the initial reaction,

$$e + A \rightarrow e + X; \quad (1)$$

where A is a nucleus in the target medium, and X is a hadronic jet produced in the initial reaction. Due to the Landau-Pomeranchuk-Migdal (LPM) effect, at UHE soft electromagnetic radiation is suppressed and most of the energy of the electron is transferred directly to the photon. Furthermore, the cross section for e^+e^- pair production drops at UHE and the hadronic interaction between the photon and the target nucleus may dominate while the electromagnetic interaction becomes negligible. The suppression due to the LPM effect becomes stronger depending on the density of the target medium. For a general overview of the LPM effect and electromagnetic suppression various media, see Ref.[19]. Furthermore, the shapes of showers may depend upon whether they are dominantly electromagnetic or hadronic [20]. Along these lines, it is also important to determine what fraction of showers are due to charmed particles. This is important for IceCube and MACRO because an increase in the number of charmed mesons in the initial reaction will increase the number of high energy muons seen in experiments, but the contribution of high energy muons is one factor used to determine the composition of cosmic rays. In addition, charmed particles contribute to the flux of atmospheric neutrinos. Thus, experiments will need to take this contribution into account in searches for diffuse astrophysical neutrinos.

Another possible source of UHE cosmic photons is the decay of extremely massive exotic particles, topological defects, and Z-burst models [21]. Particles with masses as high as 10^{26} eV may explain the observation of super-GZK energy cosmic rays [22]. Indeed, the calculations in Ref. [22] have shown, using both standard QCD and supersymmetric QCD, that a large part of the spectrum in the decay of supermassive particles consists of photons. A characteristic of these "top down" models is the existence of a large photon flux in cosmic rays. The ratio of protons to photons in the primary interaction for the production of

showers can be used to distinguish between various top-down scenarios. It is necessary, in order to address the issues above, to place upper limits on the growth of the real photon cross section. Upper limits have been placed on the fraction of primary photons at 26% [23] by analysis at the Auger observatory, but those upper limits are sensitive to the photon-nucleus interaction. The main purpose of this paper is to combine the MFGS dipole model (in the limit that the incident photon is real) with unitarity constraints and phenomenological expectations to estimate the actual growth of the real photon cross section with target nucleons/nuclei at UHE. We allow the cross section to grow with energy as fast as possible under the constraints of the S-channel unitarity, and thereby we at the very least place upper limits on the growth of photon-nucleus cross sections. It is worth emphasizing here that one cannot simply use a smooth extrapolation of the cross section to higher energies by assuming (as it is often done for the case of hadron-hadron scattering) a parameterization of the cross section inspired by the Froissart bound of the form, $\frac{N}{\text{tot}} = a + b \ln^2(s/s_0)$. A symptomatically, the photon-hadron cross section can grow faster than the rate of growth supplied by the Froissart bound due to the fact that the photon wave function is non-normalizable. In fact, as we will discuss, the rate of growth with energy of the photon-hadron cross section may be as fast as $\ln^3 E$ [24, 42].

The paper is organized as follows: In Sec. II we discuss the modifications of the MFGS model necessary to apply it to real photon-nucleon scattering. In Sec. III we evaluate the rate of growth of the γ -proton cross section at UHE and we indicate the advantages and limitations of the current approach. We estimate, within the model, the fraction of the total cross section due to the di-ractive processes and find it to be quite close to the black disk limit of 50%. We also demonstrate that nearly 25% of the total cross section at the highest energies comes from production of leading charm (the interaction of the photon in the cc component at photon energies of 10^{12} GeV). For a target ^{12}C nucleus, this ratio rises to around 30% due to differences in the degree of shadowing for charm and light quark dipoles. In Sec. IV we extend the results of Sec. III to the case of a ^{12}C target. We find that blindly extending the procedure we used for the proton target (imposing an upper limit of unity on the nuclear profile function) leads to the paradoxical result that the ratio of the nuclear and nucleon cross sections exceed the total number of nucleons, A . We explain that this is a consequence of the small thickness of the target. The main result of our investigations is the general observation that tuning is necessary for the elementary cross sections of the

hadronic subprocesses in γ -N scattering, and that, due to the large amount of diffractive scattering for the hadronic subprocesses in γ -N scattering, there is a significant amount of shadowing in γ -A scattering. We develop and we summarize our results in the conclusion. In App. A we indicate the parameterization that we used to extrapolate the gluon parton density to extremely small x , and in App. B we give a general description of the energy dependence of UHE cross sections based on the properties of the photon wave function and energy dependence of the dipole-nucleon interaction.

II. THE PHOTO-PRODUCTION LIMIT

In the perturbative QCD dipole model, the total (virtual) photon-nucleon cross section due to the interaction of the small size configurations with a target is written as the convolution product of a basic perturbative cross section for the interaction of the hadronic Fock component of the photon with the transverse and longitudinal light-cone wave functions of the photon, $j_{T,L}(z;d)$, see e.g. Refs. ([10, 43]):

$$j_{T,L}^N(x;Q^2) = \int_0^1 dz \int d^2d j_{T,L}(z;d) j_{tot}(d;x^0); \quad (2)$$

If the 4-momentum of the incident photon is q , then, in the conventional notation, $Q^2 = q^2$. Of course, the longitudinal component of the photon wave function vanishes in the limit that the photon is real, $Q^2 \neq 0$, and the transverse component becomes a unique function of the quark momentum fraction, z , and the hadronic size, d . The transversely polarized photon's light-cone wave function is,

$$j_T(z;d) = \frac{3}{2^2} \sum_{q=1}^{n_f} e_q^2 [(z^2 + (1-z)^2)^2 K_1^2(d) + m_q^2 K_0^2(d)]; \quad (3)$$

where the sum is over n_f active quark flavors, m_q is the quark mass, the K 's are the modified Bessel functions of the second kind, e_q is the fractional charge of quark q , and $z^2 = Q^2(z(1-z)) + m_q^2$. (See Ref. [26] for discussion of appropriately dealing with quark masses.) For UHE photons, Eq. 3 will include a term for the light quarks ($m_q \approx 3$ GeV) as well as a term for charm ($m_q \approx 1.5$ GeV). More massive quarks are strongly suppressed by the light-cone wave function and are neglected in the present analysis (but see Sec. III for more discussion of the heavier quarks). The energy dependence in Eq. 2 enters through the

Bjorken- x variable is only used in deep inelastic scattering:

$$x = \frac{Q^2}{2P \cdot q};$$

where P is the 4-momentum of the target nucleon. The MFGS model specifies the small size and large size cross sections and a scheme for interpolating between the two. In the original formulation of the MFGS model [13], x and Q^2 are taken as input for the calculation of a particular cross section. Note in Eq. 2 that the value of Bjorken- x , x^0 , used in the basic dipole-nucleon cross section is not the same as the external value of Bjorken- x . A relationship between x and x^0 must be supplied by the specific model, and for the MFGS model x^0 is an effective average Bjorken- x for the dipole-nucleon scattering subprocess. For a detailed derivation of the relationship between x and x^0 , see Ref. [13]. For our purposes we may quote the result:

$$x^0 = \frac{Q^2}{2P \cdot q} \left(1 + \frac{4m_q^2}{Q^2} \right) \left(1 + \frac{0.75}{d^2(Q^2 + 4m_q^2)} \right); \quad (4)$$

The model is well-defined (finite) in the photo-production limit, $Q^2 \rightarrow 0$; but the external value of x vanishes for all energies when $Q^2 = 0$ and is clearly not appropriate as input to the basic cross section. Rather, we would like to $x|Q^2 = 0 = 0$ and specify E . To this end, we note how the original value of x^0 used in Ref. [13] behaves for $Q^2 \neq 0$:

$$x^0|Q^2 \neq 0 = \frac{4m_q^2}{2P \cdot q} \left(1 + \frac{0.75}{4d^2m_q^2} \right); \quad (5)$$

The constant, d , relates the size of the hadronic configuration to the virtuality, Q^2 , of a particular quantum fluctuation of the photon through the relation, $Q^2 = -d^2$. The method of calculating x^0 used in Eq. 4 is derived for the small size components of the photon where the photon fluctuates into a $q\bar{q}$ pair which then exchanges a single gluon with the target. Note that, even when $x \neq 0$, the effective value, x^0 , is large when $d \neq 0$.

In the original formulation of the MFGS model, the large size configurations were characterized by growth with energy that mimicked the $\ln^2(\frac{W^2}{W_0^2})$ growth of the pion-nucleon total cross section with $W_0^2 = 400 \text{ GeV}^2$ (or $x_0 = 0.01$ for DIS kinematics). That is, it was assumed in Ref. [13] that for large sizes,

$$(x^0; Q^2) = \pi_N(x^0; Q^2) = 23.78 \text{ mb} \frac{x_0^{0.08}}{x}; \quad (6)$$

This behavior for the pion cross section was extracted from data in Ref. [27]. Furthermore, soft pomeron exchange leads to a factor of $e^{\frac{0.7d^2}{d^2} \ln(\frac{x_0}{x})}$ with $x_0 = 25 \text{ GeV}^2$ and $d = 65 \text{ fm}$.

in the scattering amplitude. In the case of the virtual photon discussed in Refs. [13, 14], the external value of x was used for the large size behavior. Clearly, this is inappropriate in the photo-production limit where $x = 0$.

In fact, we will now argue that the appropriate value of x to use for the large size configurations is the same x^0 (Eq. 4) that was used for the small size behavior in Ref. [13]. To see this, consider the large W^2 , fixed q^2 , limit of the pion-nucleon scattering cross-section (considering, for the moment, q to be the pion 4-momentum):

$$\begin{aligned} W^2 &= (q + P)^2 \\ &= M^2 + 2P \cdot q + q^2 \\ &\stackrel{x \neq 0}{=} 2P \cdot q; \end{aligned} \tag{7}$$

Then,

$$\begin{aligned} \ln \frac{W^2}{W_0^2} &= \ln \frac{2P \cdot q}{2P \cdot q} \\ &= \ln \frac{x_0}{x} + \ln \frac{Q^2}{Q_0^2}; \end{aligned} \tag{8}$$

where Q_0 is defined so that $x_0 = Q_0^2 / (2P \cdot q) = 0.01$. If we regard the pion mass as a particular value for the photon virtuality, then we see that Eq. 8 generalizes to any small photon virtuality Q^2 and small Bjorken scaling variable, x . On the other hand, in the limit of small Q^2 and non-vanishing size, d , Eqs. 4, 5 and 8 yield,

$$\ln \frac{x_0^0}{x^0} = \ln \frac{2P \cdot q}{2P \cdot q} \tag{9}$$

$$= \ln \frac{W^2}{W_0^2}; \tag{10}$$

where x_0^0 corresponds to taking $Q \neq Q_0$. In other words, to truly mimic the behavior of the pion-nucleon cross section, one should use the effective Bjorken- x that was used in sampling the gluon distribution. Comparing Eqs. 8 and 10, we also have

$$\ln \frac{x_0^0}{x^0} - \ln \frac{x_0}{x} = \ln \frac{Q^2}{Q_0^2}; \tag{11}$$

Thus, if one uses the external values of x in Eq. 6 then one overestimates the large size cross section by a factor of $(Q_0^2/Q^2)^{0.08}$ which diverges in the limit of a real photon. Finally, we can determine the value of x_0^0 by noting that $W_0^2 = 400 \text{ GeV}^2$ implies $Q_0^2 = 4 \text{ GeV}^2$.

Therefore, from Eq. 5, we have,

$$x_0^0 = x_0 (1 + m_q^2) \quad 1 + \frac{75}{4d^2 (1 + m_q^2)} \quad : \quad (12)$$

The second term, m_q^2 , in parentheses in Ref. 12 is implicitly divided by 1 GeV^2 so that it is unitless. Notice that the difference between x_0 and x_0^0 is only significant for small d or large m_q . The conclusion of this section is that it is appropriate to use the effective x^0 given in Eq. 4 for all values of Q^2 and that Eq. 4 must be used in the photo-production limit. Furthermore, x^0 is calculated unambiguously from Eq. 5 and Eq. 4 and with the condition that the target nucleon is at rest so that $P_q = M_E$. For the rest of this paper, we assume that the target nucleon is at rest and we specify E as input for the dipole model of the real photon.

III. GROWTH OF THE CROSS-SECTION AT VERY HIGH ENERGIES

When one considers the profile function as in Ref. [14], or the S-matrix as is done in Ref. [15], one finds that the unitarity constraint is usually violated at very low values of Bjorken- x (Ultra-High Energy). This sort of behavior is evidence of breaking of the leading twist approximation and indicates the onset of qualitatively new QCD phenomena. However, the small size configurations of the UHE real photon wildly violate the unitarity constraint due to the rapid growth of the perturbative expression,

$$\hat{A}_{pQCD}(d; x^0) = \frac{2}{3} d^2 \hat{g}_s(Q^2) x_0^0 g_N(x^0; Q^2); \quad (13)$$

at small x^0 even when the increase of the radius of the interaction with energy is taken into account. Therefore, it becomes necessary to introduce some new assumptions about the unitarity violating components of the total cross section in order to make some sense of the UHE behavior. We choose to adhere to the usual assumption that at UHE, in the region where small size perturbative methods begin to break down, the cross section is at (or near) the limit set by unitarity. This assumption is supported by our studies of the amplitudes of the dipole-nucleon interaction at HERA energies [14]. For reference, the hadron-proton amplitude that was used in Ref. [14] and which we use in this paper is given by,

$$F_{hN}(s; t) = i s \hat{A}_{tot} \frac{1}{(1 - t/M^2(d^2))^2} \frac{1}{1 - t d^2 = d^2 m_q^2} e^{\frac{0 d^2 t}{d^2} \ln \frac{x_0}{x}}; \quad (14)$$

with,

$$M^2(d^2) = \begin{cases} 8 & m_1^2 (m_1^2 - m_0^2) \frac{d^2}{d^2} ; d \neq d \\ m_1^2 & ; \text{otherwise} \end{cases} \quad (15)$$

(See Ref. [14] for the detailed procedure for obtaining this.) For these equations, $m_1^2 = 1.1 \text{ GeV}^2$, $m_0^2 = 0.7 \text{ GeV}^2$ and $m_2^2 = 0.6 \text{ GeV}^2$. The typical size of the pion is $d = 0.65 \text{ fm}$, x^0 is 0.25, and $x_0 = .01$.

Very large size configurations tend not to violate the unitarity constraint in a gross way – the total cross section for large size configurations increases slowly with energy, but there is suppression of the impact parameter at small b with increasing energy due to diffusion consistent with the Donnachie-Landshoff soft Pomeron [28]. In fact, the fit of [28] does violate S-channel unitarity for LHC energies and above. However, this leads to a very small effect for the total cross sections for the energies we discuss here. We can enforce the unitarity assumption about the high energy behavior if we re-calculate the total photo-production cross section by using the basic cross section of the MFGS model with linear interpolation everywhere except where the unitarity limit is violated. When the unitarity limit is violated, we set the cross section equal to the maximum value allowed by unitarity. More specifically, we first decompose the basic cross section in terms of the impact parameter representation of the amplitude (usually called the profile function) using the optical theorem. Let $F_{hN}(E; b)$ be the hadron-nucleon amplitude and let b be the 4-momentum exchanged in the subprocess. Then, we calculate,

$$F_{\text{tot}}^N(E) = 2 \int_0^Z dz \int_0^Z d^2d j_T(z; d) j^2(d^2; b; d); \quad (16)$$

where $j(E; b; d)$ is the profile function for a configuration of size d . The hadronic profile function that we use is given by the usual definition,

$$j(E; b; d) = \frac{1}{2\pi(2)^2} d^2 b e^{ib} F_{hN}(E; b); \quad (17)$$

so long as it is less than one. If it exceeds unity, then we explicitly reset $j(E; b; d) = 1.0$. Note that in the limit of $d \rightarrow 0$, both x^0 and the photon wavefunction become mass independent. As we shall see, the distribution of hadronic sizes involved in the interaction becomes more and more sharply peaked around small sizes as $E \rightarrow 1$. Thus, in the UHE limit, the sum in Eq. 3 will contain significant contributions from all massive strongly interacting particles. The energies that we consider in this paper are still not high enough to

Light Quark Contribution

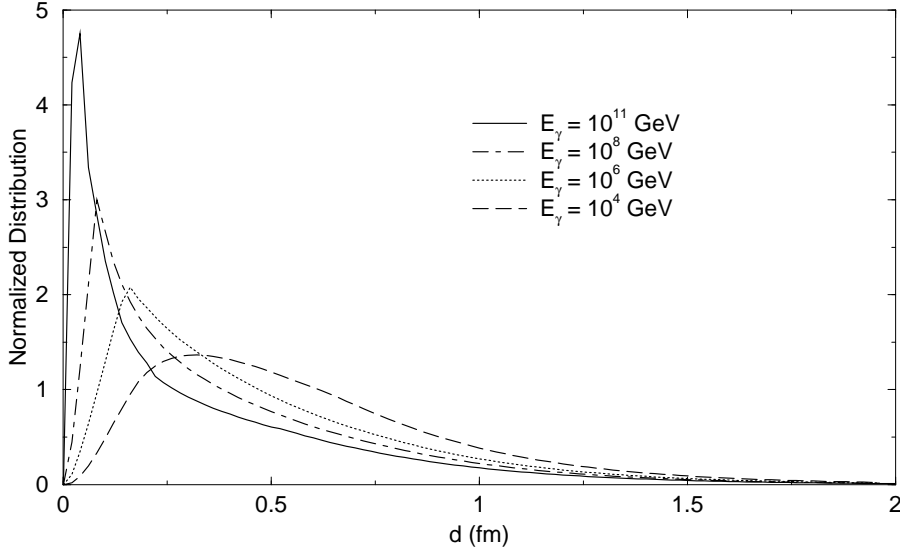


FIG. 1: The distribution of the integrand in Eq. (2) over hadronic sizes. Here, the unitarity constraint, $\Gamma = 1$, is explicitly enforced. Nevertheless, the distribution becomes sharply peaked around small hadronic sizes for UHE photons.

include all heavy particles, but, as we will discuss, there is a significant charm contribution. We include the charm contribution in the calculation of the cross section and note that the resulting hadronic showers will likely consist of a significant number of charm ed particles like D^0 mesons. The contribution from the bottom quark will be suppressed relative to the charm due to its larger mass and smaller electromagnetic coupling. We neglect the contribution from bottom and all heavier particles.

In our calculations, we use CTEQ 5L gluon distributions [29]. We note that, since significant sections of the matching region will violate the unitarity constraint, then trying to achieve an extremely smooth interpolation is an arbitrary modification to the model which achieves no genuine improvement. For simplicity, therefore, we use the linear interpolation in the MFGS model. The plots in Figs. 1 and 2 demonstrate the resulting distribution of hadronic sizes in the photon. Naturally, the peak at small sizes becomes sharper in the UHE limit.

Before leaving the subject of t -dependence in the UHE photon, we recall that in the original MFGS model of the t -dependence, discussed in Ref. [14], the diffusion of the small size $q\bar{q}$ pairs was neglected. However, in a recent overview [30] of the behavior of hadronic

Charm Quark Contribution

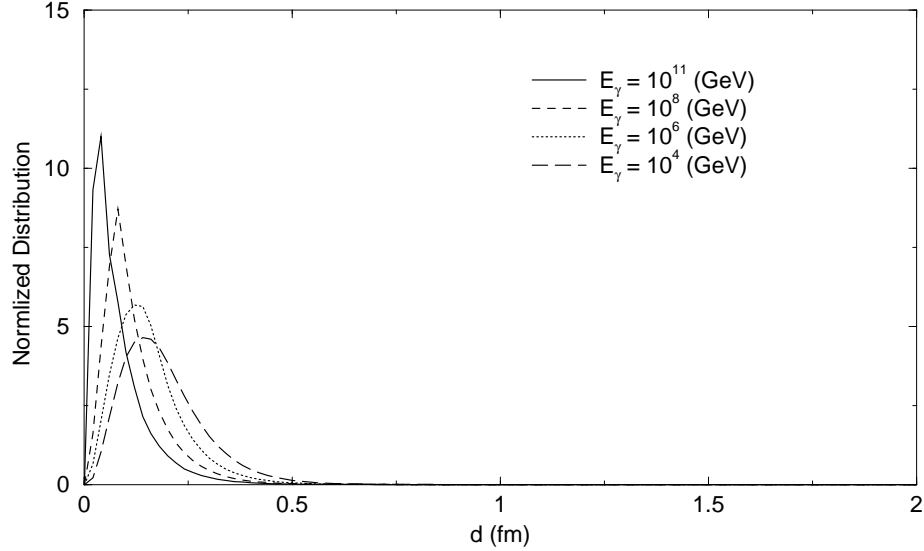


FIG. 2: This is the distribution of the charm contribution normalized to one. Comparing with Fig. 1, we see the suppression of massive quark contributions. Comparing this with Fig. 1, we see that the distribution for heavier quarks is more sharply peaked around small transverse sizes relative to lighter quarks.

cross sections at UHE, the maximum diusion of small size configurations at UHE was considered. In order to correct for the small size diusion, we slightly modify the diusion factor in the amplitude of Ref. [14] to the form,

$$F^P(t; x) = e^{^0(d) \frac{t}{2} \ln(x_0 = x)}; \quad (18)$$

where $^0(d) = 25(1 - 0.5e^{18d^4}) \text{ GeV}^2$. For sizes, d , greater than the pion size ($d = 65 \text{ fm}$), the value of 0 quickly approaches the usual slope ($^0 = 25 \text{ GeV}^2$) in accordance with the Donnachie-Landshoff soft Pomeron as in Ref. [14]. However, unlike the Regge slope in Ref. [14] which vanishes at small sizes, the value of 0 approaches 125 GeV^2 for $d = 2 \text{ fm}$, which is the diusion rate for small size dipoles determined recently in Ref. [30]. The use of the exponential function ensures that the interpolation through the transition region is continuous, and that 0 approaches 25 GeV^2 rapidly for $d \approx 65 \text{ fm}$ and 125 GeV^2 for $d = 2 \text{ fm}$. Note that at very high energies we should take into account that the Fourier transform of $F^P(t; x)$ should contain a tail / $\exp(-b)$ for some mass scale, b . However, in the energy range discussed in this paper it is a small effect and hence we neglect it.

Samples of the profile function obtained when we use the above t -dependence and the

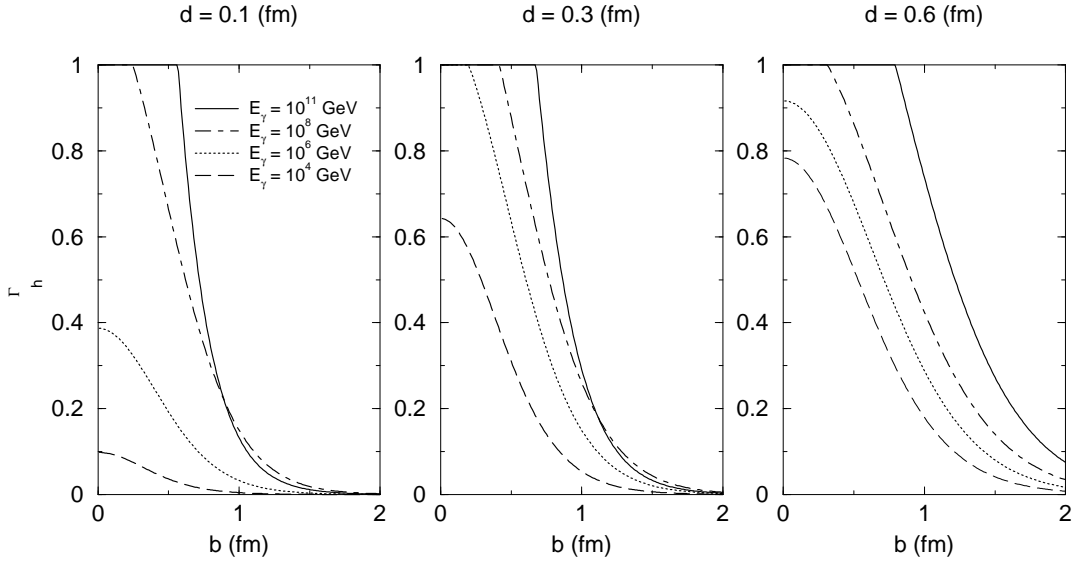


FIG. 3: Samples of the profile function for the hN interaction for real photon energies of 10^4 GeV (dashed line), 10^6 GeV (dotted line), 10^8 (dot-dashed), and 10^{11} GeV (solid line) for a range of hadronic sizes.

above procedure for taming the unitarity violations are shown in Fig. 3. Note the extremely rapid growth with energy at sizes of $d = 1$ fm.

γ -proton cross section

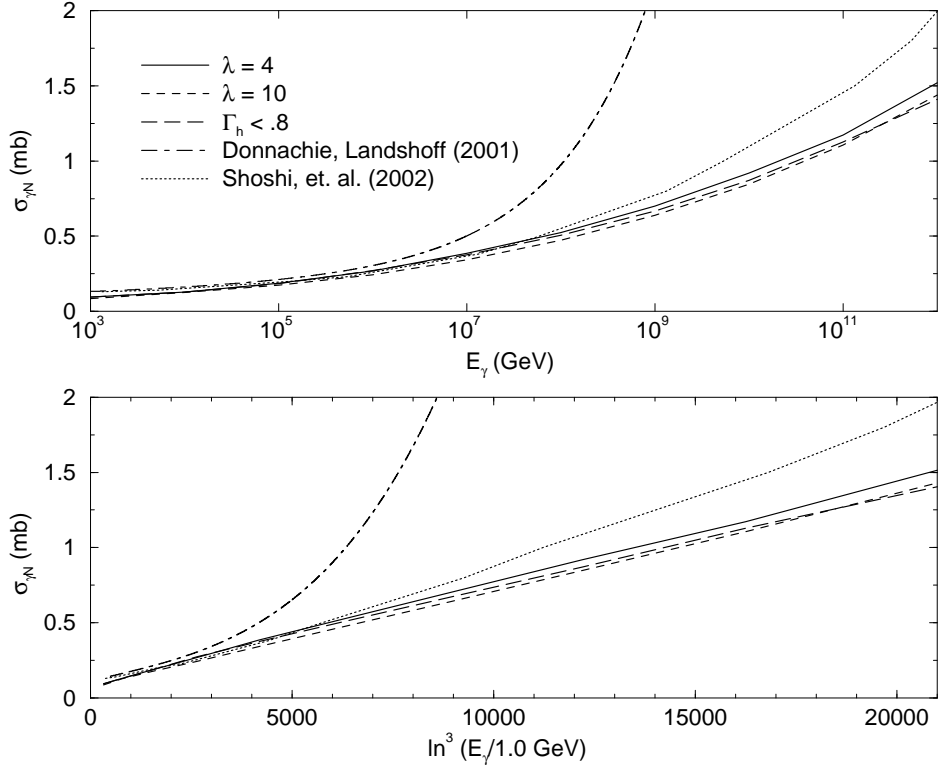


FIG . 4: G rowth of the total photon nucleon cross section for the range of energies from $E = 10^3$ GeV to $E = 10^{12}$ GeV . On the x-axis of the bottom panel, $\ln^3(\frac{E}{E_0})$ ($E_0 = 1.0$ GeV) is plotted to allow for easy comparison with the expected energy dependence at UHE (see App. B). The lowest three curves in each panel are the result of using the M FG S m odel with variations in m odel dependent parameters to demonstrate numerical sensitivity (see text). For comparison, the upper curve shows the two Pom eron m odel of D onnachie and Landsho Ref. [31] and the dotted curve shows the m odel of Shoshi et. al Ref. [16].

The procedure described above may be regarded as placing an upper limit on the growth of the cross section since we have taken the maximum contribution that does not violate unitarity. The resulting nucleon cross section has been plotted in Fig. 4. To test the numerical sensitivity to a variation in the upper limit of the profile function, we have included the result of placing the upper limit of the profile function at 0.8 rather than at 1.0. In the studies [10, 13] the matching parameter, λ , was estimated based on the analysis of the expressions for $\Gamma_L(x; Q^2)$ to be of order 10. A later analysis of the $J=$ production [32] suggested that a better description of the cross section for the intermediate $0.5 \leq d \leq 0.3$ fm is given by $\lambda = 4$ while the cross section in the perturbative region depends very weakly on

. We therefore include in Fig. 4 the result of using $\gamma = 10$ to test the sensitivity to the matching ansatz. It is evident that variations in these parameters make a small reduction in the upper limit. For the rest of this paper, we assume that $\gamma = 4$ and that the unitarity constraint implies, $h = 1$.

For comparison, the Donnachie-Landshoff two-Pomeron model [31] with no unitarity constraint is also shown in Fig. 4. Yet another approach was used for calculations in Ref. [16]. The result of this calculation is shown as the dotted curve in Fig. 4. In the model of Ref. [16], the large size components are modeled by non-perturbative QCD techniques, but the small size components use a Donnachie-Landshoff two-Pomeron model with parameters somewhat different from the original model. While the method used in Ref. [16] imposes in part parameter space unitarity in the dipole picture, it does not account for the non-normalizability of the photon wavefunction. Instead, a unitarity constraint is imposed upon the S -matrix for γ -proton scattering, and is thus less restrictive than our approach which applies unitarity constraints to the profile function for individual hadronic configurations. Our approach thus restricts the growth of the cross section more than either of the two above scenarios as can be seen in Fig. 4.

It has been observed that agreement with data is improved if one uses $M_S \bar{N} LO$ pdfs in very low- x DIS experiments. Our main concern is that the rate of increase described by the interpolation that we obtained in Eqs. A 1-A 3 of the appendix is not drastically modified by the inclusion of higher order effects. In particular, the rate of growth, and the order of magnitude of higher order corrections should not be drastically altered from what one obtains at leading order. To argue that this is the case, we notice that the LO and NLO parton densities grow at nearly the same rate at very high energies. This is demonstrated for a typical small configuration size in Fig. 5 where we compare the LO and NLO CTEQ 5 parton densities lowest values of x where parameterizations exist. The main difference between the two parton densities is that, in the high energy limit, the leading order gluon density is nearly a constant factor larger than the NLO pdf. (This makes sense when one considers the color factor 9/4 difference between quark-antiquark dipoles, and gluon dipoles and the need to include $q\bar{q}g$ dipoles in a consistent NLO formulation of the dipole model.) Indeed, above about $E = 20000$ GeV in the plot of Fig. 5, the LO curve is shifted by about a constant factor of 9/4 upward from the NLO curve, and the energy dependence used (see Eq. A 2 of App. A) describes both curves with an accuracy of $\sim 10\%$ for the energy range

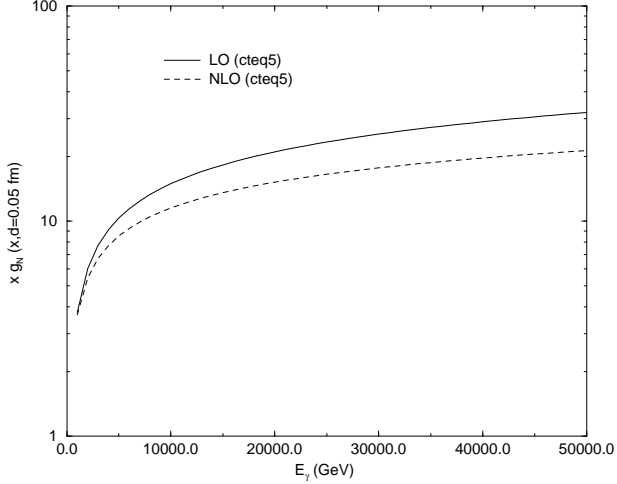


FIG. 5: Plot comparing the growth of LO and NLO pdfs at high energy for the small dipole size, $d = .05 \text{ fm}$.

$E_\gamma > 20,000 \text{ GeV}$. In the spirit of obtaining an upper limit on the growth of the cross section, we continue to use the LO pQCD result. Since we checked that our LO inspired parameterization of $(d; x^0)$ describes the data well down to $x = 10^{-3}$ the difference in the normalization is likely to be partially absorbed in the definition of the cross section. Note also that the recent studies of the small x behavior of the gluon densities indicate that the NLO approximation is close to the resummed result down to $x = 10^{-7}$, see a review in [33].

Before leaving the discussion of the nucleon target, we note several advantages and disadvantages of the current approach: First, we note that Fig. 4 is consistent with the rate growth of the cross section for a real photon at UHE which we find in App. B to be $\ln^3(E/E_0)$, where E_0 is of order 1 GeV (see e.g. [28] for a review of the Froissart bound for the hadron-hadron scattering cross section, See App. B for a generalized discussion of energy dependence for real photons.)

We are also able to analyze the contribution from different avors separately. In Fig. 6, we see that the fraction of the total cross section due to charmed particles rises to nearly 25% at 10^{12} GeV . This indicates that a large fraction of showers initiated by UHE photons should contain a pair of leading charmed particles. It is worth investigating whether such showers have a substantially longer penetration depth in the atmosphere and could be separated by the Auger detector.

Furthermore, by recalling the relationship between the diffractive component of the basic

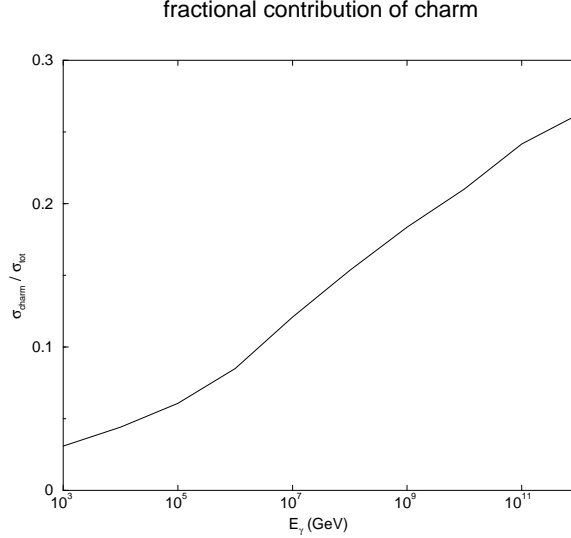


FIG . 6: The fraction of the total hadronic γ -proton cross section due to charm $q\bar{q}$ pairs.

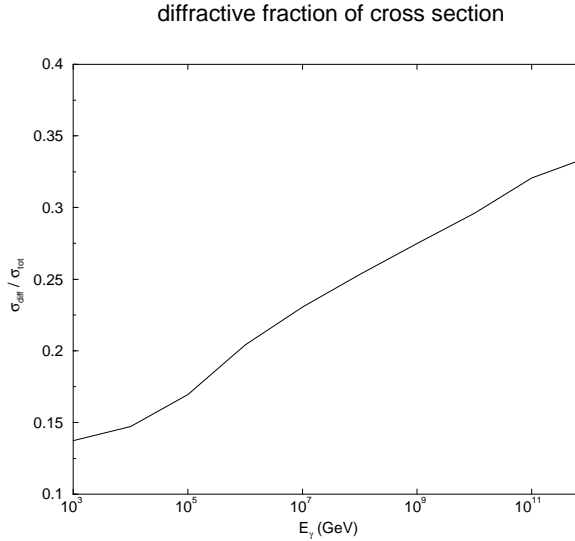


FIG . 7: The fraction of the total hadronic γ -proton cross section due to diffractive reactions of the hadronic component. The large fraction of the cross section due to diffractive scattering at $E_\gamma = 10^{12}$ GeV indicates relative nearness to the black disk limit.

cross section, $\hat{\sigma}_{diff}$ and the hadronic profile function,

Z

$$\hat{\sigma}_{diff} = \frac{d^2 b}{d\theta^2} j_h(\theta)^2; \quad (19)$$

we may also separate the fraction of the total hadronic profile function due to diffractive scattering. This is shown in Fig. 7, which gives a integrated measure of the proximity to the black disk limit. In the black disk limit, diffractive scattering accounts for exactly half of the total cross section. Therefore, the fact that, as Fig. 7 shows, the fraction of the cross section

due to diffractive scattering is around .35 at UHE indicates that diffractive scattering plays a significant role and that there will be large shadowing in nuclei.

Since the cross section grows extremely quickly at UHE, then the unitarity limit is saturated even at values of dipole size around $d = 0.1 \text{ fm}$. Figure 1 demonstrates that the largest contributions to the total photo-production cross section come from regions around $d = 0.1 \text{ fm}$ and from the transition region. Sizes smaller than this contribute very little to the total cross section. Thus, pQCD provide very little detailed information, since all models of the basic cross section (at small sizes) which violate the unitarity constraint at $d = 0.1 \text{ fm}$ will give very similar results. Furthermore, since the gluon distribution rises very sharply between $d = 0 \text{ fm}$ and $d = 0.1 \text{ fm}$ at very high energies, then the calculation in Eq. 2 becomes more sensitive to how the gluon distribution is sampled. Thus, there is more sensitivity to the parameter, α , used to relate the hadronic size to the hardness of the interaction. As seen in Fig. 4, if $\alpha = 10$, then the cross section is suppressed by around ten percent from its value when $\alpha = 4$.

The largest source of theoretical uncertainty comes from the region of large hadronic sizes. Though the behavior of large configurations can be reasonably expected to follow pion behavior at accelerator energies, we do not have any experimental data for $\sim 10^6 \text{ GeV}$ hadrons with which to model these extremely high energy Fock states. Moreover, we have so far been associating each hadronic Fock state with a particular size. It may be that as the energy of the photon increases, a large number of hadronic Fock states (perhaps multiple pion states) may be associated with a single size. Moreover, contributions from large impact parameters become significant for extremely energetic photons. Thus, predictions become sensitive to how the model handles the t -dependence of the amplitude. The current model is based on the assumption that the typical t -dependence for low energies continues into the UHE regime. Note, however, that in the case of the pp scattering the analysis of [30] indicates that, though the black disk limit leads to the slope $B / \ln^2 s$, this is a very small correction for the energies discussed here. Finally, we want to emphasize that we allow the impact parameter amplitude to approach $\alpha = 1$ without a slowdown at $t = 0.5$ as happens in many other dipole models where eikonal type parameterizations of the dipole-nucleon cross section are used (see, for example, [34]). Therefore, our approach yields a conservative upper bound.

IV . N U C L E A R T A R G E T S

Since we are interested in the interaction of UHE photons with atmospheric nuclear targets, we now go on to investigate the growth of the UHE cross section for the case of a real photon scattering from a nuclear target. The steps apply to any of light nuclei constituting the atmosphere, but we use ^{12}C for the purpose of demonstration since the ^{12}C nucleus has the approximate number of nucleons for a typical atmospheric nucleus.

At first glance it seems natural to repeat the procedure we followed for the proton case in Sec. III with the profile function given by a nuclear shape, and cross section for the interaction of the small dipoles as given by Eq. (12). However we found that if we follow this procedure we end up with the obviously wrong result that in the UHE limit, this approach quickly leads to the situation that $A_p \gg A_N$ which is physically unreasonable. The reason for this becomes clear if we visualize the relationship between the proton PDF and the nuclear PDF. The unitarity condition is not sensitive to effects of transverse correlations of the partons. The unitarity constraint would tame the dynamics if one could assume that the nucleus is a perfectly homogeneous distribution of nuclear matter. At high energies, the disk of nuclear matter "seen" by the incident hadronic configuration blackens as represented schematically in Fig. 8. Any inhomogeneity in the distribution of nucleons is accounted for at low energies in the grayness of the nuclear disk without yielding a quantitative difference in the total cross section. However, the actual distribution of nuclear matter in light nuclei "seen" by the incident dipole probably looks more like that of Fig. 9 – a collection concentrated regions of nuclear matter which individually grow black in the high energy limit but far apart from each other transversely. If the nuclear system is dilute and nucleons do not overlap transversely, the use of the $(b) < 1$ condition becomes insufficient. Thus, we will certainly find that $A_p \gg A_N$ if we assume that both the disk of the individual nucleon and the disk of the nucleus grow black in the high energy limit. That is, the cross section resulting from Fig. 9(b) is certainly larger than the sum of the cross sections from each of the blackened nucleons seen in Fig. 8(b). The simplest illustrative example would be to consider scattering off the deuteron – in this case neglect of the cluster structure of the system would grossly overestimate the maximum cross section for the interaction of this system with a small dipole. It is worth emphasizing that all these considerations are valid for the light nuclei and are likely to be a correction for the scattering of sufficiently heavy nuclei. A more meaningful

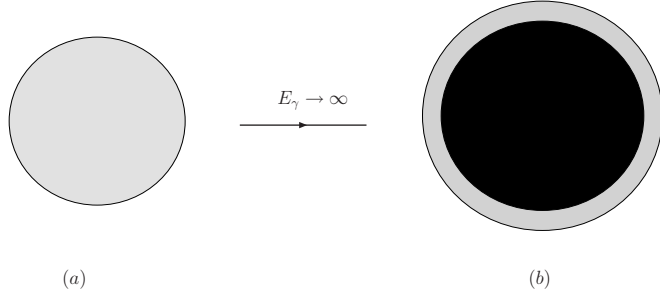


FIG . 8: The nuclear disk as 'seen' by the incident hadronic configuration in the simple homogeneous model of the unintegrated nuclear PDFs. The level of absorption by the disk is indicated by the level of grayness. At low energies, (a), the disk is weakly absorbing and homogeneous. At very high energies in (b) the disk becomes black and is thus totally absorbing.

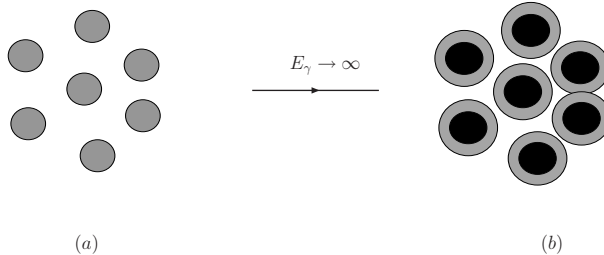


FIG . 9: A more accurate way to visualize what the incident hadronic configuration probably actually 'sees'. The nucleus consists of nucleons separated over a large distance with concentrated nuclear matter in (a). At very high energies (b), each of the nucleons becomes totally absorbing (black).

upper estimate of the cross section of scattering on light nuclei is, therefore, to take into account first the taming of the elementary cross sections and next the Glauber - Gribov theory of nuclear shadowing due to diffraction [35, 36] which does not rely on the twist decomposition of the cross section. Since we observed that diffraction constitutes a large fraction of the total cross section we expect that a large shadowing effect will emerge with growing energy. Consequently, our result will automatically be consistent with S-channel unitarity.

Hence, we use the usual approach to nuclear scattering with hadronic fluctuations, when the product of the nuclear optical density with the basic cross section is small: $\sigma_N T(b) < 1$. Starting with any standard treatment of cross section fluctuations (e.g. [37]) it can be shown

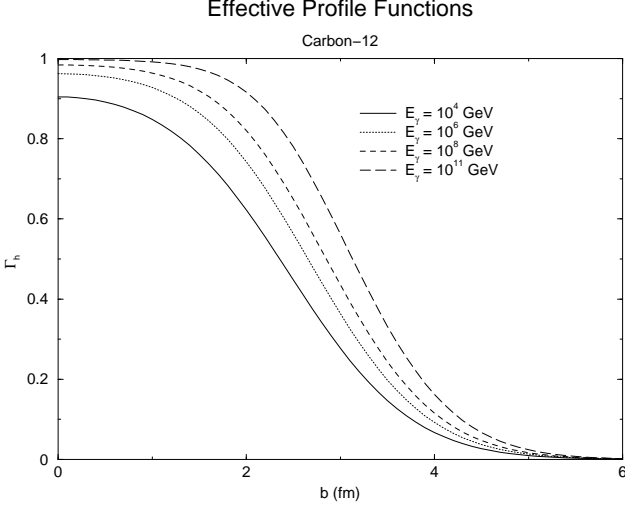


FIG. 10: Sample of the effective profile functions (see Eq. 23) for a real photon on a ^{12}C target.

that, if A_{eff} is defined by the relation, $A_{\text{eff}} = A_{\text{eff}}|_N$, then

$$\frac{A_{\text{eff}}}{A} = \frac{2 \int_0^R d^2 b (1 - e^{-\frac{1}{2} \text{eff} T(b)})}{\text{eff}}; \quad (20)$$

where,

$$\text{eff} = \frac{h^2 i}{N}; \quad (21)$$

Of course, by definition we have,

$$h^2 i = \int_0^Z dz \int_0^Z d^2 d j_T(z; d) j_{\text{tot}}^2(d; x^0); \quad (22)$$

If we write the effective profile function now as,

$$\text{eff}(b) = \int_0^Z d^2 b (1 - e^{-\frac{1}{2} \text{eff} T(b)}); \quad (23)$$

then we see that both the effective profile function and the shadowing ratio are less than unity by construction [44]. We have used the standard Fermi step fit for the nuclear optical density in Eq. 23. (Note that the diffractive components have mass squared proportional to $1-d^2$ and therefore correspond to rather large hadron multiplicities.) The result of evaluating Eq. 20 and solving for the A cross section is shown in Fig. 11. One can see that the energy dependence of the ^{12}C scattering cross section is substantially weaker than for the proton target due to nuclear shadowing, though the increase of the cross section as compared to the energies studied experimentally is still large. Since there is less shadowing for the case of incident charm dipoles, then our analysis indicates that there is a larger fraction of the

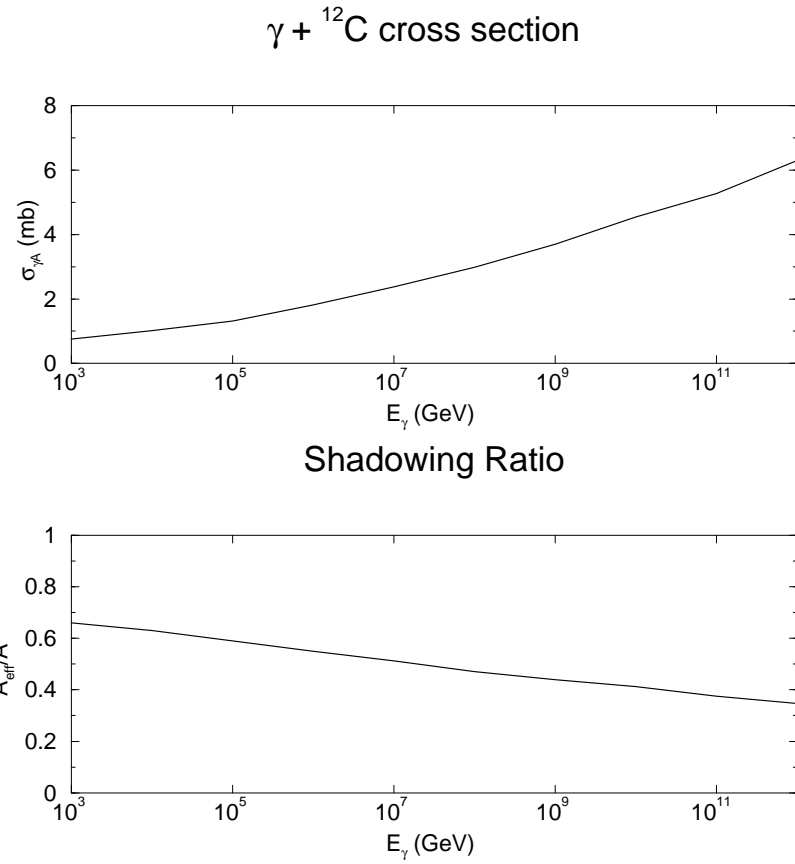


FIG .11: The upper panel shows the dependence of the ${}^{12}\text{C}$ cross section on the incident photon energy. The lower panel shows the dependence of the shadowing ratio $A = (A - A_{\text{N}})$.

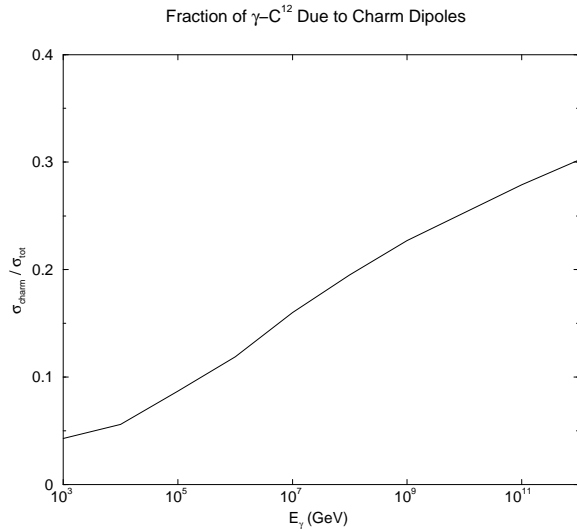


FIG .12: The fraction of the total ${}^{12}\text{C}$ cross section due to charm dipoles.

total photon- ^{12}C cross section that arises due to charm dipoles than in the case of a proton target. This is shown in Fig. 12. In the case of a target ^{12}C nucleus, the fraction of the total cross section due to charm dipoles is around 30%. The large amount of shadowing that we find already has implications for energies around 100 TeV which are relevant to a number of current cosmic ray experiments [38]. In addition, the forthcoming studies of ultra-peripheral heavy ion collisions at the LHC would allow, to some extent, a check of our predictions by measuring shadowing for photon-heavy ion interactions for the range of values for $\frac{p}{s}$ from 100 GeV to 2000 GeV. Within our model, we find that $A_{\text{eff}} = A/3$ for $\frac{p}{s} = 100 \text{ GeV}$ and $A_{\text{eff}} = A/2$ for $\frac{p}{s} = 2000 \text{ GeV}$ with $A = 220$. In order to allow for a simple extrapolation from the shadowing ratio, $(A_{\text{eff}}/A)_c$, for Carbon to other nuclei with masses typical of atmospheric atoms we use the function,

$$\frac{A_{\text{eff}}}{A} = \frac{A_{\text{eff}}}{A_c} \left(\frac{A}{12} \right)^n; \quad (24)$$

where we then determine n for a set of fixed photon energies and for the range of atomic masses, 12 to 16. As a sample, we list the following: For $E = 10^{12} \text{ GeV}$, we find $n = 1/41$; for $E = 10^9 \text{ GeV}$, we find $n = 1/35$; and for $E = 10^6 \text{ GeV}$, we find $n = 1/3$.

V. CONCLUSION

In this paper we have investigated the photon-proton/nucleus cross section in the range of energies from 10^3 GeV to 10^{12} GeV . Figure 4 demonstrates that the total cross section rises by about a factor of 12, but that there is a significant amount of uncertainty involved when the details of the model are varied. This result, however, gives us a very reasonable upper limit on the cross section since we have consistently taken the maximum cross section allowed by unitarity. The cross section varies approximately linearly with $\ln^3(\frac{E}{E_0})$ (see App. B). We use $E_0 = 1.0 \text{ GeV}$ which is consistent with hadronic sizes; see, for example, page 18 of Ref. [28].

The solid curve in Fig. 4 provides a reasonable estimate (or if we prefer to take a more cautious attitude, an upper limit) to the N cross-section at extremely high photon energies. We note that the dipole approach is consistent with the direct extrapolation of the photon-nuclear cross section [39] and with a model based on unitarity in the t-channel [40], but not with the model of [31] which uses a two-Pomeron approach and places no unitarity

constraint on the growth of the cross section. There is also disagreement with the model of Ref. [16] which uses the Donnachie-Landshoff two-Photon approach, but applies a unitarity constraint to the S-matrix for π -proton scattering rather than to the profile function of individual hadronic components.

We have shown in Fig. 6 that as much as 25% of the cross section may be due to charmed mesons for the case of a target proton, and this fraction rises to 30% when we consider a target ^{12}C nucleus. For the ^{12}C target, we use a direct application of the usual Gribbov-Glauber theory, and we find that there is a large amount of shadowing increasing with energy. It is worth noting here that though our results for the elementary π -p cross section are rather close to the results of [41] for $\frac{p}{s} = 10^3 \text{ GeV}$ considered in this paper using a generalized vector dominance model with a point-like component in the photon wave function, the model of Ref. [41] leads to a nuclear shadowing effect which is practically energy independent.

This is consistent with the dipole-proton interaction approach to the black disk limit. The resulting cross section is shown in Fig. 11 which indicates a rise in the cross section of about a factor of 7 when the energy increases from 10^3 GeV to 10^{12} GeV . The relevance of these observations is in the characterization of atmospheric showers induced by UHE neutrinos and super-GZK cosmic rays, where upper limits on the allowed growth of the photon-nucleus cross section are needed.

Acknowledgments

We would like to thank Vadm Guzey for discussions on the use of the nuclear parton distribution functions. Much of the introductory material related to cosmic ray implications arose directly from discussions with Spencer Klein and Venya Berezhinsky and we thank them for their valuable input. We would also like to thank Ralph Engel and Markus Risse for very valuable discussions. This work is supported by DOE grants under contract DE-FG 02-01ER-41172 and DE-FG 02-93ER 40771.

APPENDIX A : INTERPOLATION TO VERY SMALL BJOORKEN-X

In order to further extrapolate the basic, small size, cross section to extremely small values of x , we make a fit to the CTEQ 5L gluon distribution in the region of lowest x ($10^{-5} > x >$

10^{-4}) where the parameterizations exist. We find that the following interpolation agrees to within a few percent over the range of small x and for $0.1 \text{ fm} > d > 2 \text{ fm}$:

$$x g_N(x; d) = a(d) x^{c(d)} \quad (A1)$$

$$c(d) = -28d^{-11} \quad (A2)$$

$$a(d) = 3.9 - 13.9d + 20.1d^2 + 5 \ln d \quad (A3)$$

APPENDIX B : LIMITS ON ENERGY DEPENDENCE AT ULTRA-HIGH ENERGIES.

It is possible to obtain the general energy dependence, $\ln^3 E$ for the hadron cross section in the UHE limit within the dipole model. Here we give a general proof based only on the following assumptions about the UHE limit:

The dipole model for a finite number of active quark flavors holds for the real photon in the UHE limit.

A given finite size hadronic Fock component of the real photon scatters with exactly the maximum possible cross section allowed by the unitarity constraint when $E \gg 1$, and the rate of increase of the cross section for each individual Fock component of size, d , is limited by the rate of growth in the Froissart limit.

The very small size hadronic Fock components of the real photon scatter with a cross section whose rate of growth is no faster than a power of x^0 (or E^{-1}).

The second bullet above requires some clarification. Usually, the Froissart bound is only applied to the interaction between two hadrons rather than to the interaction between a wave-packet and a hadron. However, since the derivation of the Froissart bound is based on analyticity in the t-channel which leads to the requirement that the amplitude in impact parameter space falls off at least as fast as $e^{-2m/b}$ [28] then the argument works in our case as well [45].

We are only interested in the variation of the cross section with energy. Therefore we will leave out overall factors in order to simplify the argument. Note that $\ln \frac{x^0}{x_0}$ can always be separated into a sum of $\ln(E)$ and terms that only depend on d . For the rest of this

section, we will always write $\ln \frac{x^0}{x_0^0}$ as $\ln(E)$ since it is the leading powers of photon energy that will interest us. To be concise, the symbol \wedge will indicate how a cross section varies with photon energy, E , whereas $/$ will indicate how a cross section varies with hadronic size, d . The first of the above assumptions allows us to state that,

$$\langle E \rangle \int_0^Z d^d d \int (d) j^2 \wedge (d; x^0) : \quad (B1)$$

The integral over momentum fraction from Eq. 2 is assumed to be implicit. Also, for the rest of this section, the sum over flavors in Eq. B1 will be understood and left out. Since the energy dependence of the integrand in Eq. B1 can be understood in the extreme limit of $d \rightarrow 0$ or $d \rightarrow 1$, but is model dependent in the intermediate range of d , then let us separate Eq. B1 into the sum of three terms:

$$\langle E \rangle \int_0^Z d^d d \int (d) j^2 \wedge (d; x^0) + \int_0^Z d^d d \int (d) j^2 \wedge (d; x^0) + \int_0^Z d^d d \int (d) j^2 \wedge (d; x^0) : \quad (B2)$$

Call the terms in Eq. B2 regions 1, 2, and 3 respectively. For any given range of photon energies, one can choose sufficiently large and sufficiently small, that regions 1 and 3 must give a negligible contribution to the over-all cross section. We will justify this statement now.

First, in region 1, the cross section for the subprocess has the following behavior due to the first and last bulleted assumption above:

$$\wedge_1 (d; x^0) \sim d^2 \langle E \rangle ; \quad (B3)$$

where \wedge_1 is some positive real number. Furthermore, the light cone wavefunction of the photon gets its energy dependence from the leading behavior of the modified Bessel functions in Eq. 3. In the limit of $d \ll 1 = m_q$, $j^2(d) \sim 1/d^2$. Hence, in the limit defined by region 1, we have the following general energy dependence:

$$\text{region 1} \int_0^Z d^d d \frac{1}{d^2} d^2 \langle E \rangle \sim d^2 \langle E \rangle^{+1} : \quad (B4)$$

Next we consider the other extreme: $d \rightarrow 1$. Away from $d = 0$, Eq. B3 shows that the cross section, $\wedge(d; x^0)$ for the subprocess rises very quickly to values that violate the unitarity constraint since E is very large at UHE. At a certain value of d , the growth of $\wedge(d; x^0)$ with d must level out. Within the dipole model, the growth of $\wedge(d; x^0)$ is at with respect to variations in the transverse size of the hadronic component in the limit that d is large. Call

the upper limit of the basic cross section, $\hat{\sigma}_{\max}$. Also, for $d \gg 1$, the Bessel functions give $j(d) \approx \frac{e^{-2m_q d}}{d}$. The energy dependence of the large size cross section can grow no faster than $\ln^2 E$ due to the Froissart bound (the second bulleted assumption above). Thus, for region 3 we have,

$$\text{region 3} \quad \int_1^{\infty} \frac{e^{-2m_q d}}{d} \hat{\sigma}_{\max} \ln^2(E) \approx e^{2m_q} \ln^2 E : \quad (B5)$$

For a particular range of photon energies, we may always choose m_q small enough, and d large enough that regions 1 and 2 give a negligible contribution to the total overall integral in Eq. B2. From now on, assume that m_q and d are chosen so that regions 1 and regions 2 are defined to be negligibly small. Due to the general properties of the dipole model there is always a very small contribution from very large hadronic sizes ($d > 1$) that grows slowly with energy ($\ln^2 E$), and there is always a small contribution from very small hadronic sizes whose contribution may grow very quickly (as a power of E) due to the fact that there will always be a contribution from extremely small sizes whose value of $\hat{\sigma}(d; x^0)$ has not yet reached the unitarity limit at a given photon energy. We will obtain the rate of growth of the cross section that results from assuming that the cross section attains the maximum value allowed by unitarity for the largest range of sizes possible within the general constraints of the dipole model. Regions 1 and 3 give negligible contributions to the total integral, as discussed above, and the values of $\hat{\sigma}(d; x^0)$ will be assumed to saturate the unitarity constraint for all values of d outside of range of region 1. This means that for region 2, the basic cross section (denoted by a subscript 2) has reached the maximum allowed value, $\hat{\sigma}_{\max}$, in terms of its growth with d , and the rate of growth with E is the maximum allowed by the Froissart bound. The cross section appearing in the integrand of region 2 then becomes,

$$\hat{\sigma}_2(d; x^0) = \hat{\sigma}_{\max} \ln^2 E : \quad (B6)$$

However, the requirement that region 2 contains all of the unitarity saturating contribution demands that we allow $\hat{\sigma}_2$ to have some energy dependence. This is because, as Eq. B3 shows, the basic cross section at small sizes may have as much as a quadratic d -dependence and potentially very rapid energy dependence. Therefore, at a small but fixed value of d , the basic cross section quickly rises from small values to unitarity violating values with increasing energy. However, region 1 by definition contains only the suppressed part of the integrand near $d = 0$, whereas the unitarity saturating region should be associated entirely

with region 2. As the energy of the photon is increased, therefore, we must continuously redefine region 1 so that the integrand of region 1 is confined to a smaller and smaller region around $d = 0$. This sort of behavior does not exist at $d \gg 1$, because at such large values of hadronic size, the cross section only increases as $\ln^2 E$ and there is almost no variation with hadronic size. Therefore, is defined without any energy dependence (may be given weak energy dependence, but that will only result in subleading powers of $\ln E$ in the final result.) Equation B 3 tells us that the maximum rate at which may decrease at small d is,

$$(E) \propto E^{(1+)} : \quad (B7)$$

We thus write region 2 as,

$$\text{region 2} = \int_{(E)}^{\infty} d^3d \frac{1}{d^2} \hat{\alpha}_{\text{max}} \ln^2 E \propto \ln^3(E) \quad (B8)$$

Here we have continued to use $1=d^2$ behavior for the squared photon wavefunction because this yields the fastest possible rate of divergence of the wavefunction at the lower end of the integral and thus yields the most conservative upper limit. Notice that after having given energy dependence, Eq. B 4 becomes,

$$\text{region 1} = \int_0^{(E)} d^3d \frac{1}{d^2} d^2 \ln^2(E) \propto E^{(1+)} : \quad (B9)$$

Thus we have established the behavior of each of the regions in Eq. B 1. Regions 1 yields a vanishing contribution to the total integral as $E \rightarrow 1$ and region 3 has energy dependence $\propto \ln^2 E$ whereas region 2 has energy dependence $\propto \ln^3(E)$. Taking the leading behavior in Eq. B 1 therefore gives,

$$(\text{hadron} \rightarrow \text{hadrons}) \cdot \text{Constant} \propto \ln^3 E : \quad (B10)$$

Equation B 10 applies for each active flavor individually and thus for the sum of flavors. A possible way that the rate of growth at ultra-high energies violates Eq. B 10 in spite of the unitarity limit being saturated for each flavor would be for there to be a large proliferation of new active flavors at ultra high energies.

[1] E. L. Feinberg and I. Ia. Pomerancuk, Suppl. Nuovo Cimento 3, 652 (1956).

[2] M .L.Good and W .D .Walker, Phys. Rev. 120, 1857 (1960).

[3] H .I.M iettinen and J.Pumplin, Phys. Rev. D 18, 1696 (1978).

[4] F .E .Low, Phys. Rev. D 12, 163 (1975).

[5] S.Nussinov, Phys. Rev. Lett. 34, 1286 (1975).

[6] H .Cheng and T .T .W u, Phys. Rev. 186, 1611 (1969) and previous papers of the authors.

[7] L.L.Frankfurt and M .I. Strikman, Phys. Rept. 160, 235 (1988).

[8] N .N .N ikolaev and B .G .Zakharov, Z .Phys. C 49, 607 (1991).

[9] B . Blaettel, G . Baym , L . L . Frankfurt and M . Strikman, Phys. Rev. Lett. 70, 896 (1993); L . Frankfurt, G . A . Miller and M . Strikman, Phys. Lett. B 304, 1 (1993) [arX iv:hep-ph/9305228]; L . Frankfurt, A . Radyushkin and M . Strikman, Phys. Rev. D 55, 98 (1997) [arX iv:hep-ph/9610274].

[10] L . Frankfurt, W . Koepf and M . Strikman, Phys. Rev. D 54, 3194 (1996) [arX iv:hep-ph/9509311].

[11] A .H .Mueller and B .Patel, Nucl. Phys. B 425, 471 (1994) [arX iv:hep-ph/9403256].

[12] K .G odel-B iemat and M .W ustho , Phys. Rev. D 59, 014017 (1999) [arX iv:hep-ph/9807513].

[13] M .M cDermott, L .Frankfurt, V .Guzey and M .Strikman, Eur. Phys. J. C 16, 641 (2000) [arX iv:hep-ph/9912547].

[14] T . Rogers, V . Guzey, M . Strikman and X . Zu, Phys. Rev. D 69, 074011 (2004) [arX iv:hep-ph/0309099].

[15] S . Munier, A . M . Stasto and A . H . Mueller, Nucl. Phys. B 603, 427 (2001) [arX iv:hep-ph/0102291].

[16] A . I . Shoshi, F . D . Ste en and H . J . P irner, Nucl. Phys. A 709, 131 (2002) [arX iv:hep-ph/0202012].

A . I .Shoshi, F .D .Ste en and H .J.P irner, arX iv:hep-ph/0205343.

A . I .Shoshi and F .D .Ste en, arX iv:hep-ph/0212070.

[17] S.R .K lein, arX iv:astro-ph/0412546.

[18] L.D .Landau and I.Pom eranchuk, Dokl. Akad. Nauk Ser. Fiz. 92, 735 (1953); A .B .M igdal, Phys. Rev. 103, 1811 (1956).

[19] S.K lein, Rev. Mod. Phys. 71, 1501 (1999) [arX iv:hep-ph/9802442].

[20] D .A costa et al., Nucl. Instrum . Meth. A 316, 184 (1992);
S.K lein "What do UHE Showers really look like?" Talk given at the 44th INFN E leisatron

project, Cosmic QCD at Cosmic Energies: The Highest Energy Cosmic Rays and QCD , August 29 to September 25, 2004, Erice, Italy

[21] V. Berezinsky, M. Kachelriess and A. Vilenkin, Phys. Rev. Lett. 79, 4302 (1997) [[arXiv:astro-ph/9708217](#)]; V. A. Kuzmin and V. A. Rubakov, Phys. Atom. Nucl. 61, 1028 (1998) [Yad. Fiz. 61, 1122 (1998)] [[arXiv:astro-ph/9709187](#)]; D. Fargion, B. M. Ele and A. Salis, Astrophys. J. 517, 725 (1999) [[arXiv:astro-ph/9710029](#)]; T. J. Weiler, Astropart. Phys. 11, 303 (1999) [[arXiv:hep-ph/9710431](#)].

[22] R. Aloisio, V. Berezinsky and M. Kachelriess, Phys. Rev. D 69, 094023 (2004) [[arXiv:hep-ph/0307279](#)].

[23] M. Risse [Pierre Auger Collaboration], [arXiv:astro-ph/0507402](#);

M. Risse et al., [arXiv:astro-ph/0512434](#).

[24] L. Frankfurt, V. Guzey, M. McDermott and M. Strikman, Phys. Rev. Lett. 87, 192301 (2001) [[arXiv:hep-ph/0104154](#)].

[25] V. N. Gribov, Sov. Phys. JETP 30, 709 (1970) [Zh. Eksp. Teor. Fiz. 57, 1306 (1969)].

[26] T. C. Rogers and M. I. Strikman, [arXiv:hep-ph/0410070](#).

[27] J. P. Burg et al., Phys. Lett. B 109, 111 (1982).

[28] S. Donnachie, G. Dosch, O. Nachtmann and P. Landshoff, "Pomeron Physics And QCD," Cambridge University Press, 2002

[29] H. L. Lai et al. [CTEQ Collaboration], Eur. Phys. J. C 12, 375 (2000) [[arXiv:hep-ph/9903282](#)].

[30] L. Frankfurt, M. Strikman and M. Zhalov, Phys. Lett. B 616, 59 (2005) [[arXiv:hep-ph/0412052](#)].

[31] A. Donnachie and P. V. Landshoff, Phys. Lett. B 518, 63 (2001) [[arXiv:hep-ph/0105088](#)].

[32] L. Frankfurt, M. McDermott and M. Strikman, JHEP 0103, 045 (2001) [[arXiv:hep-ph/0009086](#)].

[33] G. P. Salam, [arXiv:hep-ph/0510090](#).

[34] J. Bartels, K. Golec-Biernat and H. Kowalski, Phys. Rev. D 66, 014001 (2002) [[arXiv:hep-ph/0203258](#)].

[35] R. J. Glauber, Phys. Rev. 100, 242 (1955).
V. Franco, Phys. Rev. Lett. 24 (1970) 1452.

[36] V. N. Gribov, Sov. Phys. JETP 29, 483 (1969) [Zh. Eksp. Teor. Fiz. 56, 892 (1969)].

[37] B. Bialy, G. Baym, L. L. Frankfurt, H. Heiselberg and M. Strikman, Phys. Rev. D 47, 2761

(1993).

[38] F. Aharonian et al. [HESS Collaboration], arXiv:astro-ph/0511678; J. A. Albert et al. [MAGIC Collaboration], arXiv:astro-ph/0512283.

[39] L.B. Bezrukov and E.V. Bugaev, Yad. Fiz. 33, 1195 (1981).

[40] J. R. Cudell, E. Martynov and G. Soyez, Nucl. Phys. B 682, 391 (2004) [arXiv:hep-ph/0207196].

[41] R. Engel, J. Ranft and S. Roesler, Phys. Rev. D 55, 6957 (1997) [arXiv:hep-ph/9610281].

[42] In the case of scattering of heavy nuclei the non normalizability of the photon wave function results in $\propto_A / \ln(s=s_0)$ behavior [25].

[43] In the framework of the two gluon exchange model [4] where cross section does not depend on the incident energy the expression similar to 2 was written in Ref. [8].

[44] In principle one can write a more accurate formula which would take into account deviations of $\frac{h^n}{N}$ from $\frac{n-1}{n_{eff}}$ for $n > 3$. However numerically these effects are small especially for the light nuclei where double scattering gives a dominant contribution.

[45] Actually, in the MFGS model, the amplitude behaves as $e^{at \ln \frac{x^0}{x}}$ in the UHE limit where a is a positive constant. So, it falls off faster than $e^{-2m/b}$ in impact parameter space and therefore the cross section should not increase at precisely the maximum rate allowed by unitarity. Therefore, the fact that the MFGS model is nearly linear in $\ln^3 \frac{E}{E_0}$ in Fig. 4 indicates that pre-asymptotic effects are still significant in the considered energy range.